Spectral Methods for Resolving Spike Dynamics in the Geirer-Meinhardt Model

Michael McCourt[1,*], Nicholas Dovidio[2] and Michael Gilbert[3]

[1] *Department of Applied Mathematics, Illinois Institute of Technology, Chicago, IL 60616, USA.*
[2] *Department of Mathematics, Davidson College, North Carolina, USA.*
[3] *Department of Mathematics and Physics, Colorado State University-Pueblo, Colorado, USA.*

Abstract. The Gierer-Meinhardt reaction-diffusion model is analyzed using a spectral collocation method. This reaction-diffusion system is governed by activator and inhibitor concentrations. Initially, the system is considered in one dimension and then in two dimensions; numerical results are presented for both cases. The algorithmic complexity and accuracy are compared to those of a moving finite element method. Finally, observations are made concerning when to use the proposed spectral method as opposed to the established moving mesh method.

AMS subject classifications: 65M70

Key words: Spike dynamics, Gierer-Meinhardt model, spectral collocation.

1 Introduction

In the 1970s, Gierer and Meinhardt [6] proposed a variety of models related to biological pattern formation [23]. These models are used to describe the reactions between two substances, an activator and an inhibitor; other models have also been suggested to study pattern formation including the Schnakenberg model [25]. In this paper, a spectral collocation method is proposed to solve one such model, now called the Gierer-Meinhardt model, that describes the concentrations of the activator and inhibitor as functions of space and time. In this model, the activator is an autocatalyst, that is, it has the ability to make more of itself. In contrast, the inhibitor lives off the activator and reduces the activator's concentration. By analyzing the concentrations at different times, we can see

---

Corresponding author. Email addresses: `mccomic@iit.edu` (M. McCourt), `nidovidio@davidson.edu` (N. Dovidio), `mikey_thegr8@hotmail.com` (M. Gilbert)

how these two substances interact. Also, by altering parameters that effect the reaction speed of the two concentrations, a variety of different states can be achieved [6,22].

   The Gierer-Meinhardt (GM) model in dimensionless form is as follows:

$$A_t = \epsilon^2 \nabla^2 A - A + \frac{A^p}{H^q}, \tag{1.1a}$$

$$\tau H_t = \kappa \nabla^2 H - H + \epsilon^{-1} \frac{A^m}{H^s}, \quad x \in \Omega, \quad t > 0, \tag{1.1b}$$

$$\partial_n A = \partial_n H = 0, \qquad x \in \partial\Omega, \quad t > 0, \tag{1.1c}$$

where A is the activator concentration, H is the inhibitor concentration, ϵ is the activator diffusivity satisfying $0 < \epsilon \ll 1$, κ is the inhibitor diffusivity satisfying $\kappa > 0$, τ is the reaction-time constant, and Ω is a bounded two-dimensional domain. ∂_n denotes the normal derivative with respect to the boundary $\partial\Omega$, and x is the spatial coordinate(s). The set of exponents (p,q,m,s) satisfies

$$p > 1, \qquad q > 0, \qquad m > 0, \qquad s \geq 0, \qquad \frac{p-1}{q} < \frac{m}{s+1}.$$

   The GM model exhibits rich spike dynamics that vary depending on the parameters chosen; these spike solutions have been studied using finite element moving mesh methods described in [13, 18, 19]. Asymptotic analysis has also been applied to the spike dynamics problem to provide analytical insight into the reaction-diffusion model [8]. For the one-dimensional GM model, extensive asymptotic and numerical results have been presented for the case when $\tau = 0$, and also for $\tau > 0$ [13]. For the two-dimensional GM model there have been limited asymptotic and numerical results only for the case when $\tau = 0$. Recently, numerical results have been presented for the case when $\tau > 0$ [18,19], but asymptotic results are as yet unavailable.

   The main focus of this paper is to provide numerical results for the two-dimensional GM model for the case when $\tau > 0$ using spectral collocation. The purpose of this is to provide insight into the spike dynamics of the model, to introduce a computationally feasible way of solving spike dynamics problems, and to partially validate the results obtained in [19], since theoretical results are limited for this case. In Section 2, we outline the implementation of a Chebyshev spectral collocation method to the one-dimensional problem (2.1a), and present numerical results arising from the method. In Section 3, we show how to extend the Chebyshev spectral method to two spatial dimensions and present numerical results for the case $\tau > 0$. These results are compared to the ones in [18,19].

2   One-dimensional GM model

In one spatial dimension, the dimensionless GM model can be written as

$$A_t = \epsilon^2 A_{xx} - A + \frac{A^2}{H}, \tag{2.1a}$$

$$\tau H_t = \kappa H_{xx} - H + \epsilon^{-1} A^2, \tag{2.1b}$$

where $-1 \leq x \leq 1$ and $t \geq 0$ subject to the initial conditions

$$\begin{aligned} A(x,0) &= a_0(x), \\ H(x,0) &= h_0(x), \end{aligned} \tag{2.2a}$$

for $-1 < x < 1$ and the boundary conditions

$$\begin{aligned} A_x(\pm 1,t) &= 0, \\ H_x(\pm 1,t) &= 0, \end{aligned} \tag{2.2b}$$

for $t \in [0,T]$. The exponent set used in (2.1a) is $(p,q,m,s) = (2,1,2,0)$ and that is the only set which will be considered in this paper.

2.1 Spectral collocation method

Because our problem has non-periodic boundary conditions we will collocate algebraic polynomials rather than the trigonometric polynomials used for periodic boundary conditions [5]. This will be implemented by Chebyshev differentiation matrices; for more details, see [14]. For the spatial and temporal discretization, the following notation is used throughout this section:

$$\Phi(x,t_n) = \Phi^n, \quad \Phi(x_j,t_n) = \Phi_j^n.$$

The size of the Chebyshev matrix is determined by the number of collocation points used to solve the problem. Algebraic polynomials of high degree tend to exhibit oscillations; to counteract this we used a clustered grid determined by the Chebyshev-Gauss-Lobatto points

$$x_j = \cos\left(\frac{j\pi}{N}\right), \qquad 0 \leq j \leq N-1, \tag{2.3}$$

and N is the number of collocation points. The structure of the first order Chebyshev matrix $D \in \mathbb{R}^{N \times N}$ is :

$$(D_N)_{00} = \frac{2(N-1)^2+1}{6}, \quad (D_N)_{(N-1)(N-1)} = -\frac{2(N-1)^2+1}{6},$$

$$(D_N)_{jj} = \frac{-x_j}{2(1-x_j^2)}, \quad j = 1, \cdots, N-2,$$

$$(D_N)_{ij} = \frac{c_i}{c_j} \frac{(-1)^{i+j}}{x_i - x_j}, \quad i,j = 0, \cdots, N-1, \quad i \neq j$$

where

$$c_i = \begin{cases} 2, & i=0 \quad \text{or} \quad N-1, \\ 1, & \text{otherwise.} \end{cases}$$

By multiplying the Chebyshev matrix D by itself we find the second derivative matrix D^2.

2.2 One-dimensional GM model with a zero reaction-time constant

We now consider (2.1a) for the case $\tau = 0$, and show how Chebyshev spectral methods are implemented to evolve a one-spike solution. Setting $\tau = 0$ in (2.1a) yields the system

$$A_t = \epsilon^2 A_{xx} - A + \frac{A^2}{H}, \tag{2.4a}$$

$$0 = \kappa H_{xx} - H + \epsilon^{-1} A^2 \tag{2.4b}$$

with the same initial and boundary conditions described by (2.2b).

By discretizing in space with the set of point defined in (2.3) and applying the Chebyshev second derivative matrix D^2 to the elliptic partial differential equation (PDE) (2.4b) we find

$$0 = \kappa D^2 H^n - H^n + \epsilon^{-1} (A^n)^2,$$

where H^n and A^n are the vectors with the values of $A(x,t_n)$. The jth value in the vector is the x_j point defined in (2.3). By solving for H^n terms, it follows that

$$(\kappa D^2 - I_N)H^n = -\epsilon^{-1}(A^n)^2, \tag{2.5}$$

where I_N is the $N \times N$ identity matrix. This linear system can be solved using any number of techniques; we attempted both direct and iterative methods. Because the solution changes so little between time steps, the values of H^{n-1} provide a good initial guess of the H^n. This suggests use of an iterative method, as the required number of iterations will be low and thus overall time required will be less than a direct method. Therefore our 1D work was completed using Gauss-Seidel iterations, while LU factorization was used only to verify these results.

For the parabolic PDE (2.4a), a second-order backwards differentiation formula (BDF) was implemented to advance A^n through time. Because $\kappa \gg \epsilon^2$ (values given in Section 2.3) the impact of the spatial derivatives is vastly different, and the stiff component of this problem must be reconciled. ϵ^2 is a very small term and A_{xx} is a rapidly changing term, as can be seen in the figures, which generally indicates the need for careful handling of the solution. Analytically this multiplication of a small term with a rapidly changing term suggests singular perturbation analysis; numerically, we will need an implicit technique, hence the second-order BDF.

When applied to $u'(t) = f(t,u(t))$ the BDF gives rise to the time discretization scheme

$$u^{n+2} - \frac{4}{3}u^{n+1} + \frac{1}{3}u^n = \frac{2\Delta t}{3}f^{n+2}. \tag{2.6}$$

Applying this BDF and the Chebyshev discretization (2.3) to (2.4a) leads to the nonlinear system

$$A^{n+2} - \frac{4}{3}A^{n+1} + \frac{1}{3}A^n = \frac{2\Delta t}{3}\left(\epsilon^2 (A^{n+2})_{xx} - A^{n+2} + \frac{(A^{n+2})^2}{H^{n+2}}\right).$$

By discretizing in space using the spectral method (the Chebyshev D^2 matrix) and rearranging the system becomes

$$\left[\epsilon^2 D^2 - \left(\frac{3}{2\Delta t}+1\right)I_N\right]A^{n+2} = \frac{2}{\Delta t}A^{n+1} - \frac{1}{2\Delta t}A^n + \frac{(A^{n+2})^2}{H^{n+2}}. \tag{2.7}$$

As in the solution of (2.5), we can provide our Gauss-Seidel technique with an excellent initial guess – the solution at the previous time step. This allows the iterative method to converge in less than 10 iterations, and often less than 3 depending on the time step Δt.

Unlike (2.5), (2.7) is implicit in A^{n+2} and H^{n+2} and thus we used a fixed point iteration to find A^{n+2} by using, as an initial guess A^{n+1}. This fixed point iteration was carried out until the change between iterations is less than 5×10^{-7}. Convergence is guaranteed by the Banach fixed point theorem for

$$\left\|\epsilon^2 D^2 - \left(\frac{3}{2\Delta t}+1\right)I_N\right\|_\infty < 1.$$

2.3 One-dimensional dynamics for a zero reaction-time constant

We now consider the evolution of a one-spike solution to the one-dimensional GM model when $\tau = 0$. For this case, the dynamics of a one-spike solution to (2.1a) for $\epsilon \ll 1$ was asymptotically analyzed in [8].

In [8], the method of matched asymptotic expansions was used for $\epsilon \ll 1$ to derive the following asymptotic results for a one spike solution to the one-dimensional GM model:

Theorem 2.1. [8]: *For $0 < \epsilon \ll 1$ and $\tau = 0$, the dynamics of a one-spike solution to (2.1a) are characterized by*

$$A(x,t) \sim a_c \equiv H^\gamma w\left(\epsilon^{-1}[x-x_0(t)]\right), \tag{2.8a}$$

$$H(x,t) \sim h_c \equiv HG_m[x;x_0(t)]/G_m[x_0(t);x_0(t)], \tag{2.8b}$$

where $\gamma \equiv q/(p-1)$, and the spike location $x_0(t)$ satisfies the differential equation

$$\frac{dx_0}{dt} \sim -\frac{\epsilon^2 q}{(p-1)\sqrt{\kappa}}\left(\tanh\left[\kappa^{-1/2}(1+x_0)\right] - \tanh\left[\kappa^{-1/2}(1-x_0)\right]\right). \tag{2.8c}$$

$w(y)$ is the unique, positive solution to

$$w'' - w + w^p = 0, \quad -\infty < y < \infty; \tag{2.8d}$$

$$w \to 0 \quad \text{as} \quad |y| \to \infty; \quad w'(0) = 0, \quad w(0) > 0. \tag{2.8e}$$

In (2.8b), $G_m(x;x_0)$ is the Green's function satisfying

$$\kappa\frac{d^2 G_m}{dx^2} - G_m = -\delta(x-x_0), \quad -1 < x < 1; \qquad \frac{dG_m}{dx}(\pm 1;x_0) = 0, \tag{2.8f}$$

and the constant $H(t)$ is defined in terms of G_m by

$$H \equiv \left[\frac{1}{b_m G_m(x_0; x_0)} \right]^{1/\xi}, \qquad b_m \equiv \int_{-\infty}^{\infty} [w(y)]^m dy, \qquad (2.8g)$$

where ξ is defined by

$$\xi \equiv \frac{qm}{(p-1)} - (s+1). \qquad (2.8h)$$

Numerical experiment 1

To illustrate the Chebyshev spectral collocation method described above for solving (2.1a), we take $\epsilon = 0.03$, $\kappa = 1$, $\tau = 0$. For the remainder of this section we define

$$x_0(t) = \max_{x \in [-1,1]} \{A(x,t)\}.$$

with the initial location of the spike, $x_0(0) = 0.6$. The initial profile for A matches the initial profile used in [13],

$$A(x,0) = a_0(x) = \left(\frac{\tanh 1}{2} \right) \text{sech}^2 \left(\frac{x - x_0(0)}{2\epsilon} \right).$$

Because $\tau = 0$, Eq. (2.4b) is elliptic, and thus no initial profile for H need be chosen for this experiment.

Figs. 1-3 show the numerical solutions to (2.1a) based on our Chebyshev spectral method with $N = 128$ Chebshev spectral collocation points. In Table 1, we compare the numerical results using the spectral method with $N = 96$, and $N = 128$, with the asymptotic results and the numerical results presented in [13] using a moving mesh method. To provide a basis for comparison, we compare the results with the solution to (2.1a) using the NAG library code [12] generated in [13], using 2000 equally spaced meshpoints and strict tolerances on the time-stepping. The results should be very close to the true solution, and are shown in the last column of Table 1.

The results for the 128-point spectral method are close to the NAG library. This is indicative that our method of solution is accurate with a number of points comparable to the moving mesh method. For the purposes of this experiment, the NAG solution is taken to be the true solution; as we will realize in Section 3 the number of points required for the NAG solution in two dimensions is unwieldy and alternate methods must be considered.

This experiment is meant to test the spectral method's potential, along with the moving mesh method, as an accurate approximation to the true solution. In [20, 26] there were studies of the solution for a one-dimensional model which led to the values in the ASY column above. Analytic solutions in two dimensions are limited to the case where $\tau = 0$ with some results found in [24]. There are however no results to our knowledge of asymptotic solutions for a two-dimensional system with positive τ. This requires confirmation the accuracy of spectral collocation in one-dimension before comparing numerical solutions in two dimensions.

Table 1: Comparison of the asymptotic and numerical results for the center $x_0(t)$ of the spike $A(x,t)$.

t	$x_0(t)$ (ASY)	$x_0(t)$ (MM,200)	$x_0(t)$ (MM,100)	$x_0(t)$ (PS,128)	$x_0(t)$ (PS,96)	$x_0(t)$ (NAG)
100	0.55338	0.555	0.55	0.550	0.550	0.5506
400	0.43577	0.425	0.43	0.427	0.426	0.4272
800	0.31891	0.305	0.33	0.306	0.305	0.3064
1200	0.23441	0.215	0.23	0.219	0.219	0.2207
1800	0.14834	0.135	0.15	0.134	0.138	0.1353
3000	0.05975	0.055	0.07	0.050	0.055	0.0512

[*]Here MM denotes Moving Mesh, PS denotes Pseudo-Spectral, ASY and NAG are described in [13].
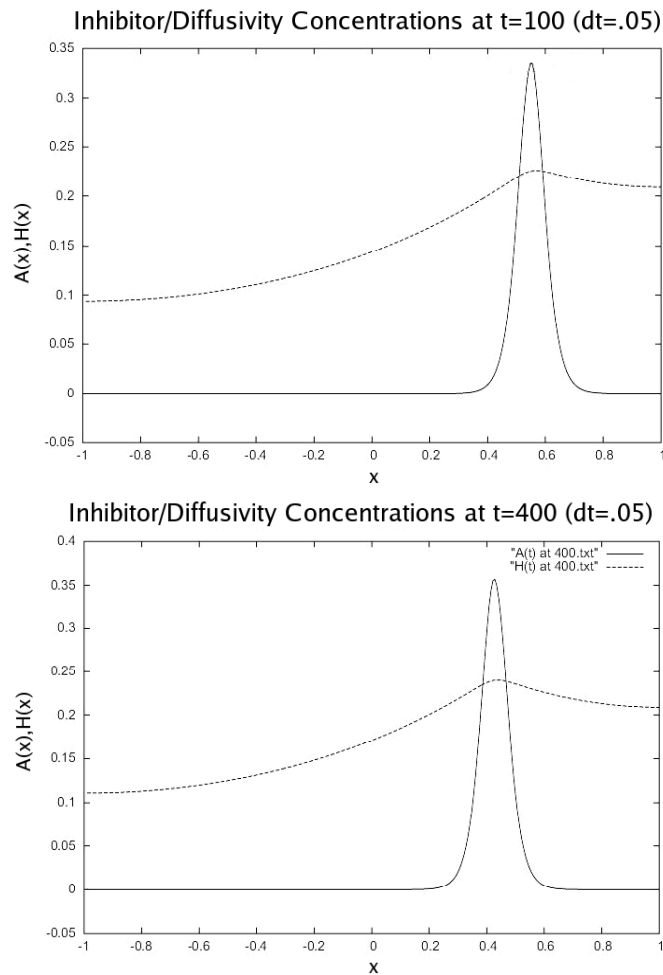
Figure 1: Activator A (solid curve) and inhibitor concentration H (dashed curve) at t=100 and t=400.

Inhibitor/Diffusivity Concentrations at t=800 (dt=.05)

Inhibitor/Diffusivity Concentrations at t=1200 (dt=.05)
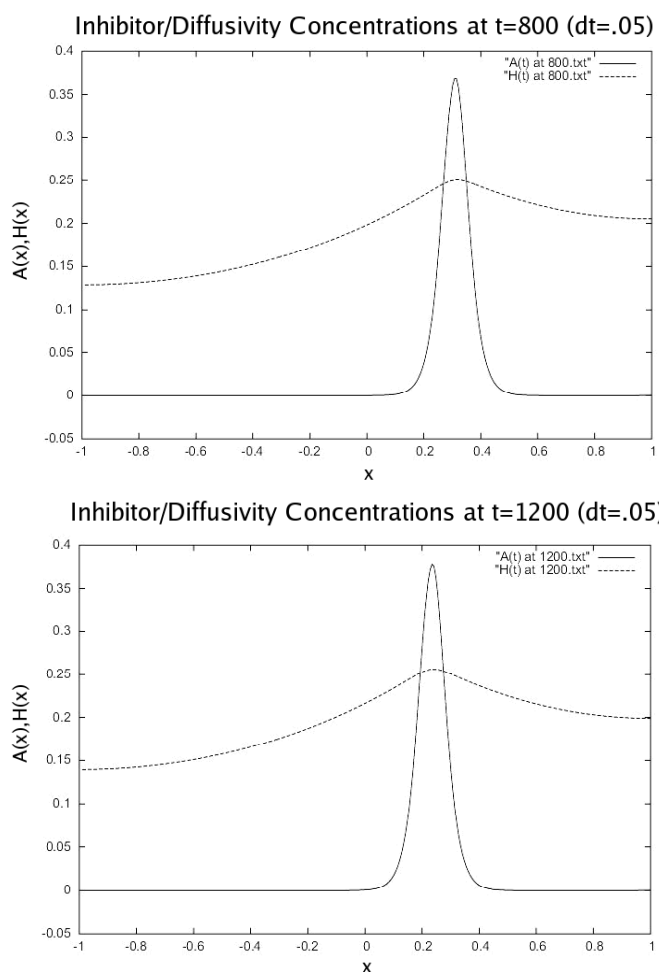
Figure 2: Activator A (solid curve) and inhibitor concentration H (dashed curve) at t=800 and t=1200.

2.4 Oscillatory dynamics with a positive reaction-time constant

In this section, we briefly discuss the oscillatory dynamics of the one-dimensional GM model for the case when $\tau > 0$. Because the H equation in (2.1a) is parabolic rather than elliptic as it is in (2.4b) we now require an initial condition for $H(x,0) = h_0(x)$. The initial profile we used was

$$H(x,0) = h_0(x) = \frac{\cosh(1-|x|)}{3\cosh(1)},$$

a form of solution to the perturbation problem (2.8b). In [13], the stability of single spike quasi-equilibrium profiles with respect to a nonzero reaction-time constant was studied. A nonlocal eigenvalue problem that determines the stability of the profile for (2.1a) was formulated, and from numerical computations of this eigenvalue problem, critical values of τ were determined for which oscillatory instabilities are triggered.
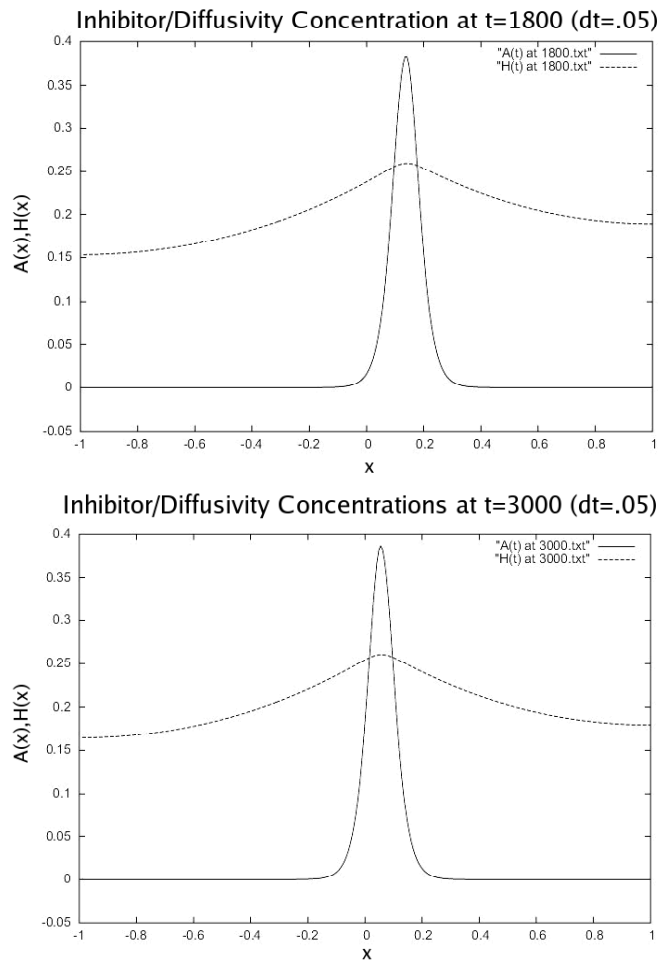
Figure 3: Activator A (solid curve) and inhibitor concentration H (dashed curve) at t=1800 and t=3000.

We briefly state these general results from [13], and then conduct a second numerical experiment using the Chebyshev spectral method for the spatial discretization in order to illustrate the efficacy of this method for the case when $\tau > 0$.

Theorem 2.2. [13]: *Assume that $0 < \epsilon \ll 1$, $\tau \geq 0$, and $x_0 \in (-1,1)$. Then, the stability of the quasi-equilibrium profile* (2.8a) *for the GM model* (2.1a) *is determined by the spectrum of the nonlocal eigenvalue problem*

$$L_0\Phi - \chi_m w^p \left(\frac{\int_{-\infty}^{\infty} w^{m-1}\Phi dy}{\int_{-\infty}^{\infty} w^m dy} \right) = \lambda\Phi, \quad -\infty < y < \infty, \tag{2.9a}$$

$$\Phi \to 0, \quad as \quad |y| \to \infty. \tag{2.9b}$$

In (2.9a), *the local operator L_0 and the multiplier χ_m are defined by*

$$L_0\Phi \equiv \Phi'' - \Phi + pw^{p-1}\Phi, \tag{2.9c}$$
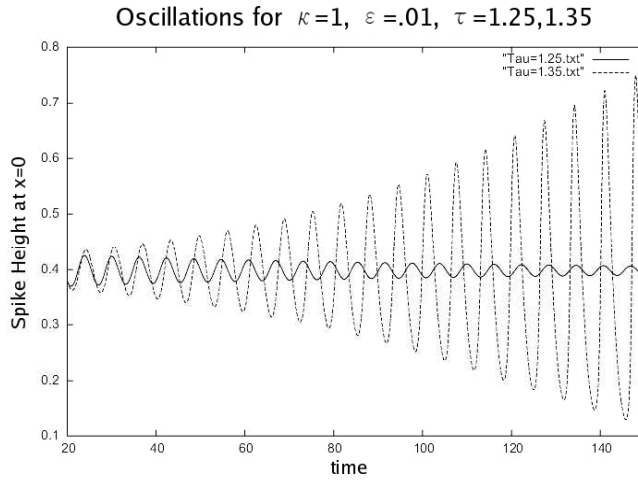
Figure 4: Plots of A_m (spike height) versus t for (2.1a) with $\tau = 1.25$ (solid curve), $\tau = 1.35$ (dashed curve).

and

$$\chi_m = \chi_m(z;x_0) \equiv qm \left[s + \sqrt{1+z} \left(\frac{\beta(\theta_\lambda;x_0)}{\beta(\theta_0;x_0)} \right) \right]^{-1}. \tag{2.9d}$$

Here the function $\beta(\xi,x_0)$ is defined by

$$\beta(\xi,x_0) \equiv \tanh[\xi(1+x_0)] + \tanh[\xi(1-x_0)], \tag{2.9e}$$

$$z \equiv \tau\lambda, \qquad \theta_\lambda \equiv \theta_0\sqrt{1+z}, \qquad \theta_0 \equiv \kappa^{-1/2}. \tag{2.9f}$$

Numerical computations were carried out in [13] in order to determine the critical bifurcation value for τ, called τ_0, for which oscillatory instabilities are observed. It was found that for (2.1a) with the initial spike location $x_0(0) = 0$, τ_0 is a monotonically decreasing function of κ. In particular, it ranges from the value $\tau_0 \approx 2.749$ when $\kappa \ll 1$, to $\tau \approx 0.771$ when $\kappa \gg 1$. Here we consider the bifurcation which occurs for $\kappa = 1$.

Numerical experiment 2

We now present a numerical solution to (2.1a) for the case $\tau > 0$. In Fig. 4 we plot the amplitude of the spike, called $A_m(t) \equiv A(0,t)$, as a function of t for three different values of τ when $\kappa = 1$ and $\epsilon = 0.01$. In particular, we plot $A_m(t)$ for $\tau = 1.25$ and $\tau = 1.35$. These results lead us to believe that the point of bifurcation τ_b is between $1.25 < \tau_b < 1.35$, as was described in [13].

It is worth noting that the rapidly oscillating results depicted here require the implicit time stepping technique described by (2.6). The slow drift to equilibrium observed in the first numerical experiment are not as demanding as these dynamics. Indeed, certain parameter values may allow us to forgo the fully implicit methods in favor of something more efficient. We will however need to be careful for future experiments that we do not assume more efficient time stepping discretization can be taken when the dynamics are oscillatory.

3   Two-dimensional GM model

In this section, we describe the implementation of the Chebyshev spectral collocation method for the two-dimensional GM model (1), and present numerical results for the case when $\tau > 0$. We then compare the results to those of [19], the only two-dimensional results known to us for the case when $\tau > 0$.

The numerical techniques for applying the spectral method are similar to those found in one dimension. Once again the technique is separated into two factors: spatial discretization and time stepping. Using the same exponent set as before $(p,q,m,s) = (2,1,2,0)$, (1.1a) becomes

$$A_t = \epsilon^2 \nabla^2 A - A + \frac{A^2}{H}, \tag{3.1a}$$

$$\tau H_t = \kappa \nabla^2 H - H + \epsilon^{-1} A^2, \tag{3.1b}$$

$$\partial_n A = \partial_n H = 0, \quad x \in \partial \Omega, \tag{3.1c}$$

for $t > 0$. In this paper, we only consider results obtained on the unit square $\Omega = \{(x,y) \in [-1,1]^2\}$. For this domain, the boundary conditions become

$$A_x(\pm 1, y, t) = A_y(x, \pm 1, t) = 0, \tag{3.2a}$$
$$H_x(\pm 1, y, t) = H_y(x, \pm 1, t) = 0. \tag{3.2b}$$

3.1   2D spectral collocation method

3.1.1   Spatial discretization

Since the boundary is a rectangle, the solutions A and H at each time step can be easily organized into a vector. We use an equal number of collocation points N in both x and y, although the methods described henceforth can be generalized to N_x points in the x dimension and N_y points in the y dimension if desired.

If the unknowns are ordered by rows, the Laplacian operator ($\nabla^2 u = u_{xx} + u_{yy}$ in Cartesian coordinates) takes the form

$$\nabla^2 \equiv I_N \otimes D^2 + D^2 \otimes I_N, \tag{3.3}$$

where $\otimes$ is the Kronecker tensor product, I_N is the $N \times N$ identity matrix, and D^2 is the previously defined second order Chebyshev differentiation matrix. As we can see from the ordering of the unknowns, the $I_N \otimes D^2$ term corresponds to the second derivative with respect to x and the $D^2 \otimes I_N$ corresponds to the second derivative with respect to y, see, e.g., [9].

3.1.2   Time discretization

Before we can continue to build our linear system we must tackle the same difficulties faced when considering time discretization in one dimension. There is a similar balance

between accuracy (implicit methods) and efficiency (explicit methods) and to optimize this algorithm we need to explore several avenues.

To maintain stability without the complexity of solving a fully nonlinear problem, we have chosen to implement the backward Euler method and retard the nonlinear terms; this will be termed a linearly implicit method. This places moderate restrictions on the stability region (and on the values of κ, τ and ϵ as described at the end of Section 2.4), but requires only one linear solve per iteration. Since our systems are now of size N^2 instead of N this is important because each linear solve is now of greater complexity. While it was computationally practical to perform a simple fixed point iteration in one dimension, doing so in two dimensions will require too much time.

For this section, we define the vector $A^n = A(x,y,t+n\Delta t)$. By applying the linearly implicit method to (3.1b) the problem becomes

$$\frac{A^{n+1}-A^n}{\Delta t}=\epsilon^2\nabla^2 A^{n+1}-A^{n+1}+\frac{(A^n)^2}{H^n},$$

$$\frac{\tau}{\Delta t}(H^{n+1}-H^n)=\kappa\nabla^2 H^{n+1}-H^{n+1}+\frac{(A^{n+1})^2}{\epsilon}.$$

By discretizing in space using the spectral method this is

$$\left[\left(1+\frac{1}{\Delta t}\right)I_{N^2}-\epsilon^2(I_N\otimes D^2+D^2\otimes I_N)\right]A^{n+1}=\frac{1}{\Delta t}A^n+\frac{(A^n)^2}{H^n}, \qquad (3.4a)$$

$$\left[\left(1+\frac{\tau}{\Delta t}\right)I_{N^2}-\kappa(I_N\otimes D^2+D^2\otimes I_N)\right]H^{n+1}=\frac{\tau}{\Delta t}H^n+\frac{(A^{n+1})^2}{\epsilon}. \qquad (3.4b)$$

The vector division in (3.4a) is term by term, which is to say the ith term is computed by squaring the ith term of A^n and dividing it by the ith term of H^n.

3.1.3 Boundary conditions

We have not yet incorporated the boundary conditions: this will be done in a similar fashion as is done for 1D, but it is more complicated in 2D.

Let us begin by considering the question of which rows should be replaced. The ith element in the vector is on the boundary if:

Table 2:

Condition	Boundary
$i\equiv 0 \bmod N$	$x=-1$
$i\equiv N-1 \bmod N$	$x=1$
$\lfloor i/N\rfloor=0$	$y=-1$
$\lfloor i/N\rfloor=N-1$	$y=1$

If there are N collocation points in each dimension then there are $N-2$ collocation equations arising from interior points. The matrices which represent the left-hand side of
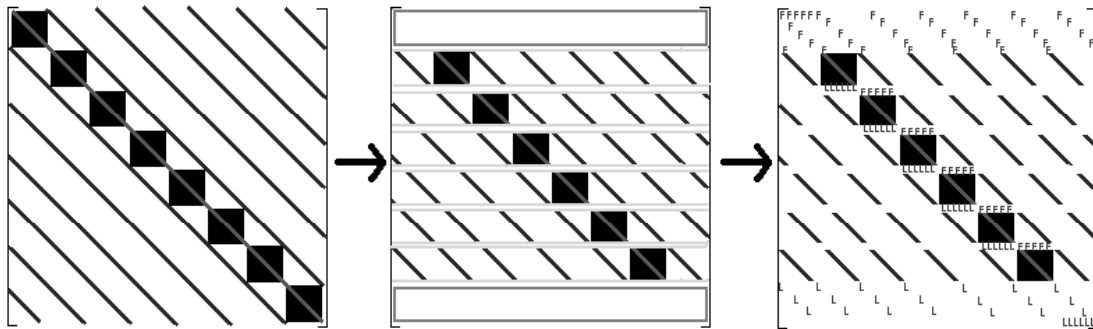
Figure 5: Matrix sparsity plot showing non-zeros, and which entries correspond to boundary values.

(3.4a) and (3.4b) have size $N^2 \times N^2$ though, which requires exactly $N^2 - (N-2)^2 = 4N - 4$ equations from the boundary points for a unique solution.

If we examine the number of rows which satisfy the conditions above, we see that there are in fact $4N - 4$ rows described; however, corner points $\{(x,y) | (|x|,|y|) = (1,1)\}$ have two boundary conditions imposed upon them simultaneously. We were unable to find a graceful way to implement both boundary conditions simultaneously, so we have chosen to consider only one boundary condition at each corner. The choices were arbitrary, with the normal x derivative imposed at $(1,1)$ and $(-1,-1)$ and the normal y derivative at $(-1,1)$ and $(1,-1)$.

Now that we know the rows which correspond to boundary values we are able to consider changing our matrix to compensate. To preserve spectral accuracy, a spectral equation must be formed, and this can be done using the Kronecker tensor product similarly to the Laplacian definition (3.3).

The x boundary conditions can be extracted from the matrix $I_N \otimes D$ and the y boundary conditions can be extracted from the matrix $D \otimes I_N$. Replacing the boundary rows indicated in Table 2 by the same rows from either $I_N \otimes D$ or $D \otimes I_N$ determined again from Table 2 we can complete this system. This transfer of rows can be seen in Fig. 5.

We will define the following notation for the matrices from (3.4a) and (3.4b) after substitution of the appropriate boundary conditions

$$\left[\left(1 + \frac{1}{\Delta t} \right) I_{N^2} - \epsilon^2 (I_N \otimes D^2 + D^2 \otimes I_N) \right] \xrightarrow{+B.C.} \mathcal{A},$$

$$\left[\left(1 + \frac{\tau}{\Delta t} \right) I_{N^2} - \kappa (I_N \otimes D^2 + D^2 \otimes I_N) \right] \xrightarrow{+B.C.} \mathcal{H}.$$

For the right-hand side vectors, applying the homogeneous boundary conditions consists of replacing the rows indicated by Table 2 with 0. The new notation is

$$\frac{1}{\Delta t} A^n + \frac{(A^n)^2}{H^n} \xrightarrow{+B.C.} b_{\mathcal{A}}^n,$$

$$\frac{\tau}{\Delta t} H^n + \frac{(A^{n+1})^2}{\epsilon} \xrightarrow{+B.C.} b_{\mathcal{H}}^n.$$

3.2 Implementation

The system we plan to solve can be described as the coupled system

$$\mathcal{A}A^{n+1} = b^n_{\mathcal{A}},$$
$$\mathcal{H}H^{n+1} = b^n_{\mathcal{H}}.$$

From this we can develop an algorithm to compute the discrete values on $t \in [0,T]$

3.2.1 The algorithm

```
Specify parameters:  N, ε, τ, κ, Δt, T
Compute first and second derivative matrices, D and D² , of size N
Construct A and H matrices:
    {I_N⊗D²} Place the D² blocks on the diagonal of A
    {D²⊗I_N} Place the D² values on the bands of A
    Copy A to H
    Multiply −ε²A and −κH
    Diagonal Add 1+τ/Δt to the H diagonal, 1+1/Δt to A diagonal
    x BC Replace x rows indicated by Table 1 with I_N⊗D
    y BC Replace y rows indicated by Table 1 with D⊗I_N
Set initial conditions of A⁰ = A(x,y,0) and H⁰ = H(x,y,0)
Step through time by Δt until T
    Calculate b^n_A from A^n and H^n
      Solve the system A^{n+1} = A^{−1}b^n_A
    Calculate b^n_H from A^{n+1} and H^n
      Solve the system H^{n+1} = H^{−1}b^n_H
```

3.2.2 Linear equation solvers

At this point, everything has been discussed except the most computationally expensive part of this process - the solution of the two linear systems per time step.

In Section 2.4, our one-dimensional systems are solved by Gauss-Seidel iterations and direct methods. When the value of Δt used is small, the previous time step is an excellent initial guess and the Gauss-Seidel method converges in five or fewer iterations. For large values of Δt, which are acceptable because we implement the fully implicit 2nd-order BDF, the initial guess is not as accurate and it becomes faster to use Gaussian elimination.

Thus we are faced with the ultimate decision: direct or iterative methods. The choice is determined by the size of the system which needs to be solved and the size of the time step. The time step logic was just explained, but the importance of the size of the system is not quite as obvious - it deals with the density of the matrix, and simply stated, as the matrix becomes less dense it tends to be more profitable to use iterative methods. See [7] or [15].
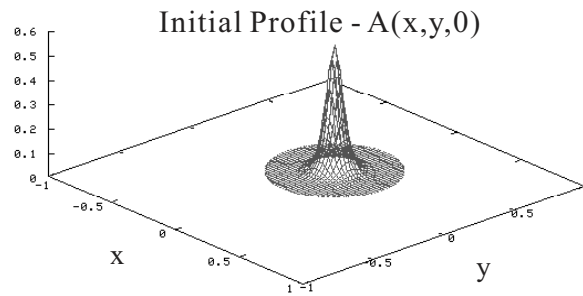
Figure 6: Initial profile for activator concentration.

If the size of the matrix is N^2, then for the 2D spectral method the fill, or ratio of nonzero entries per number of total entries, is:

$$\text{Fill} = \frac{(2N-1)(N-2)^2 + N(4N-4)}{(N^2)^2}.$$

There are $2N-1$ nonzeros per row on the interior of the domain, and N nonzeros per boundary row. When simplified, this reads:

$$\text{Fill} = \frac{2}{N} - \frac{5}{N^2} + \frac{9}{N^3} - \frac{4}{N^4}. \tag{3.5}$$

For the choice of 50 points in each dimension, we see that the matrix is $\simeq 3.9\%$ dense. For this specific problem, there is little to be gained in changing between direct and iterative methods; for less dense matrices we will use iterative methods and for more dense matrices we will use direct methods. As it turns out we will need more than 50 points to assure accuracy and therefore we will only use iterative methods, specifically GMRES with ILU(0) preconditioner. See [15] for details, and [17] for details on the implementation.

3.3 Numerical experiments

In every experiment in this section, the initial conditions implemented are

$$A(x,y,0) = \frac{1}{2}\left(1 + .001\sum_{k=1}^{20}\cos\frac{ky\pi}{2}\right)\text{sech}^2\left(\frac{\sqrt{x^2+y^2}}{2\epsilon}\right),$$

$$H(x,y,0) = \frac{\cosh(1-\sqrt{x^2+y^2})}{3\cosh(1)},$$

with $\epsilon = .04$. See Fig. 6 for the A initial profile. We will restrict ourselves with the activator dynamics in the paper. The experiments were carried out in C++.
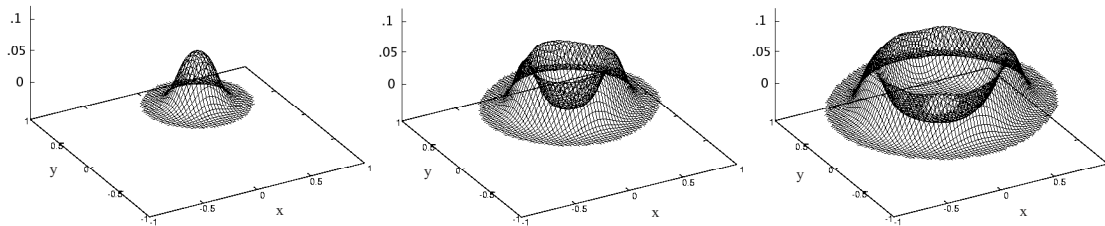
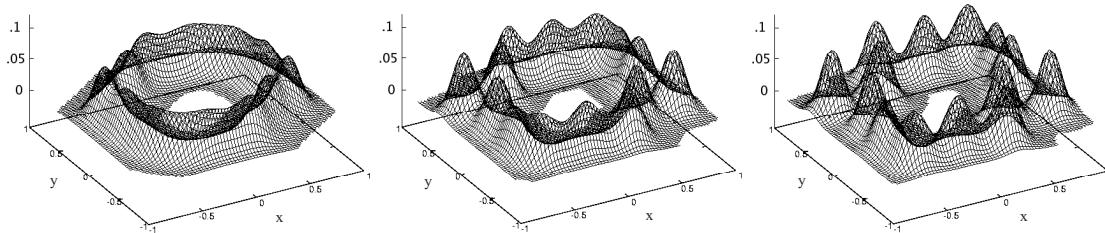Figure 7: Spike splitting with $\tau=.1$, $\kappa=.0128$, $\epsilon=.04$ at $t=20,80$ and 170.
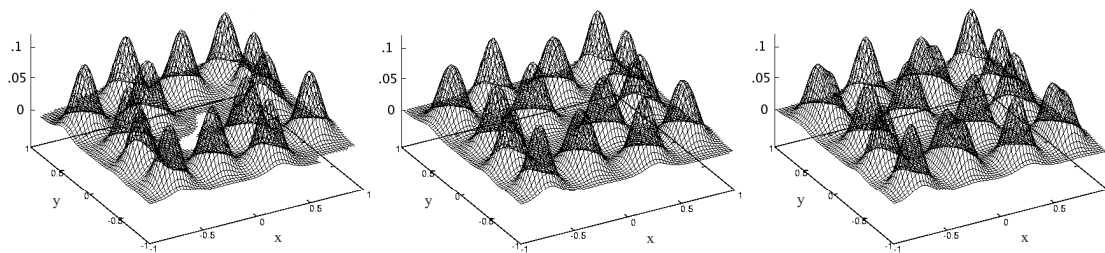

Figure 8: Same as Fig. 7, except at $t=270,320$ and 340.

Figure 9: Same as Fig. 7, except at $t=370,420$ and 440.

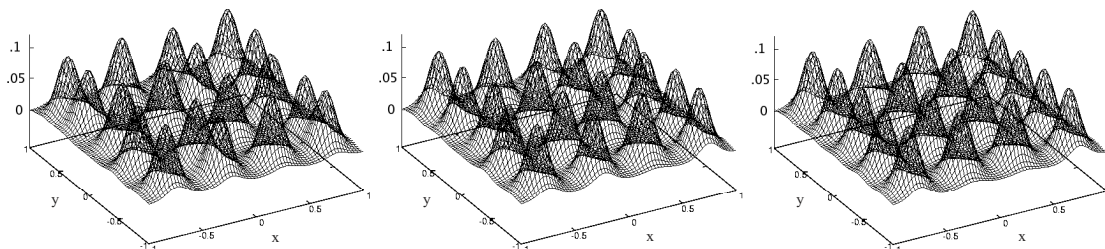Figure 10: Same as Fig. 7, except at $t=460,500$ and 900.

3.3.1 Spike splitting

In [19], Qiao theorized that given a fixed τ value, there is a κ value which will result in the two-dimensional domain filling with spikes. For $\tau=0.1$ it has been determined that values of $\kappa=\mathcal{O}(\epsilon)$ will result in spike splitting.

One such instance can be seen for $\kappa=0.0128$, where a spike of height $\sim.6$ localized at the origin deforms into a ring which expands to fill the domain. The ring then collapses
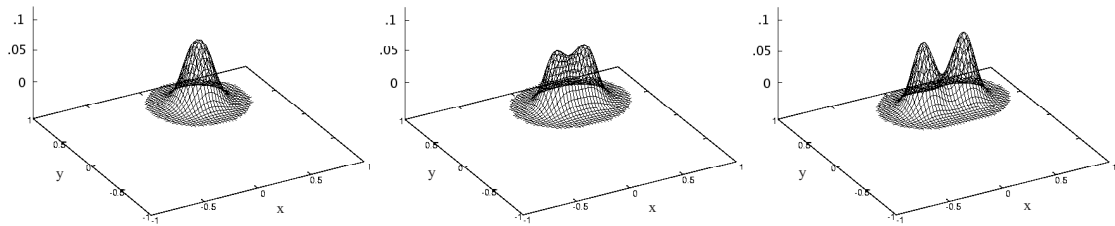
Figure 11: Spike splitting with $\tau=.1$, $\kappa=.0152$, $\epsilon=.04$ at $t=30,80$ and 90.
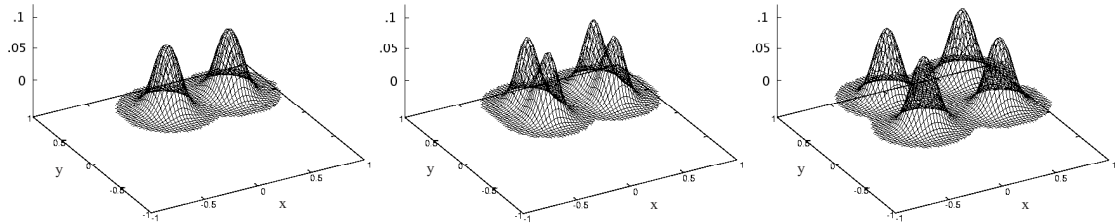
Figure 12: Same as Fig. 11, except at $t=140,160$ and 220.
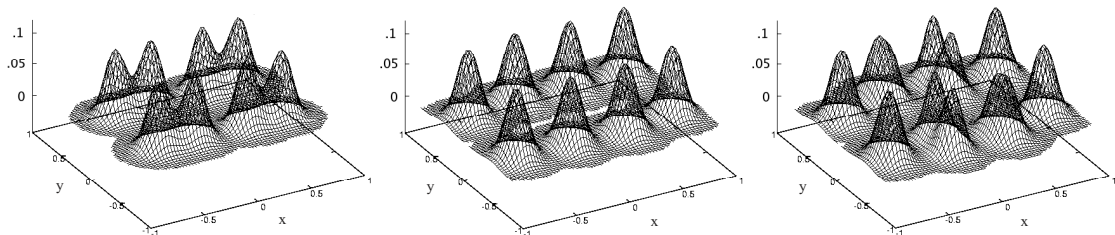
Figure 13: Same as Fig. 11, except at $t=290,520$ and 570.
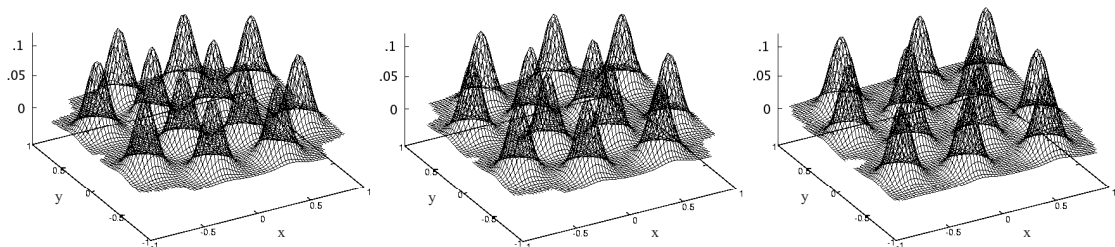
Figure 14: Same as Fig. 11, except at $t=620,750$ and 990.

into several smaller spikes and by $t=600$ the entire region is filled with spikes with height $\sim.1$. When $\kappa=0.0152$ the initial spike splits into two around $t=100$. By $t=600$, each spike has split at least twice more and the entire region is again filled with spikes, although in a different pattern than before.

The results were calculated using a reasonable time step, $\Delta t=.1$, and it was unnecessary to use a fully implicit time discretization for accurate results. When we compare the Figs. 7-14 with results for the same experiment in [19], we see that the spectral method

has provided the same results as Qiao's moving mesh method. This also confirms that values of $\kappa = \mathcal{O}(\epsilon)$ and $\tau = 0.1$ results in an initial spike located at the origin splitting and spikes filling the domain, as predicted by Qiao.

4   Conclusions

4.1   Complexity

Our current technique of using preconditioned GMRES means that each time step requires between $\mathcal{O}(N^2)$ and $\mathcal{O}(N^4)$ operations depending on how effectively we perform matrix-vector multiplication. Unfortunately, because each row has at least N nonzeros, it is impossible to achieve efficiency less than $\mathcal{O}(N^3)$. Our algorithm uses methods developed in PETSc to take advantage of the sparse structure of the matrix for GMRES and matrix-vector multiplication.

In terms of storage, the sparse representations of the matrices $\mathcal{A}$ and $\mathcal{H}$ will require 2 vectors of length N^2 ($N \times N$ matrices) to hold D and D^2. It is never actually necessary to construct the matrices $\mathcal{A}$ and $\mathcal{H}$ because the structure is known and the values in each of the matrices are comprised of only values from D, D^2 and the input parameters. Also, 4 vectors of length N^2 are needed to store $b_{\mathcal{A}}$ and $b_{\mathcal{H}}$ at the current time step and the previous time step.

It is that storage which motivated the use of the first order implicit-explicit BDF for time stepping and not the second order method as was used in one dimension. The second order method requires storing the solution at two previous time steps rather than just one, which in turn necessitates $6N^2$ memory spaces instead of $4N^2$. While this is not problematic for small N, as we increase N we reach the memory limits of the machine and therefore it is more practical to use the first-order method rather than the second-order one.

4.2   Future work

From our work we are able to confirm the numerical results presented in [18, 19] and use similar grid sizes to resolve the dynamics: 3025 for our method vs. 3066 for the moving mesh method. Because these two techniques approach the problem from very different perspectives, it is difficult to compare them. Fundamentally, both methods require nearly equal time to evolve the oscillating or steady state solutions because while the spectral method requires a smaller time step, there is a remesh requirement at each time step for the moving mesh method.

All the numerical experiments were completed on a single machine with a dual 1.7 GHz Pentium 4 Xeon processor and 2 GB RDRAM. Since we are already using PETSc for data storage and access, it is logical to attempt to move this project into parallel with the built in MPI routines. By doing so we would be able to handle more collocation points without increasing the time required to compute the solution. While we have considered

the system with $N = 99,149,199,249$ to guarantee the accuracy of the results for $N = 55$, these values are increasingly less practical for a single node. 55 points were chosen to be comparable in size to the problem size from [19].

Another improvement which can be made to this algorithm is to implement the fully implicit second-order BDF as we had in one dimension. Doing this will require solving a coupled system of nonlinear equations of size $2N^2$, probably with a Newton-like method. Such routines are provided in PETSc with the use of SNES (Structure-neutral Nonlinear Equation Solvers) objects. Hopefully this technique will allow greater freedom with the size of time step, and guaranteed accuracy for oscillating solutions in two dimensions. Qiao showed that such dynamics occurred for $\kappa = 10$, $\tau \approx .77$. These dynamics were not discussed above because accuracy cannot yet be guaranteed with the spectral method.

While the numerical results described in this paper have confirmed various one-dimensional analytic results, there is no comparison to be made to asymptotic results in two dimensions. This paper does not attempt to make conclusions about the asymptotic nature of these problems, as was done in [13] for the 1D case. Rather we have simply tried to confirm the solutions presented in [19] and extend asymptotic results from 1D to 2D. There is still a great deal of work to be done analytically - hopefully this paper will provide insight for future studies.

Acknowledgments

References

[1] U. M. Ascher, S. J. Ruuth and B. Wetton, Implicit-explicit methods for time-dependent partial differential equations, Appl. Numer. Math., 25(2-3) (1997), 151-167.
[2] R. Beauwens and L. Quenon, Existence criteria for partial matrix factorizations in iterative methods, SIAM J. Numer. Anal., 13 (1976), 615-643.
[3] S. Chandrasekaran, M. Gu and T. Pals, Fast and stable algoritms for hierachically semi-separable representations, Technical Report UCSB Math, 2004.
[4] M. Crouzeix, Une mèthode multipas implicite-explicite pour l'approximation des èquations d'èvolution paraboliques, Numer. Math., 35 (1980), 257-276.
[5] G. Fasshauer, Lecture notes from numerical differential equations, 30-32, Illinois Institute of Technology (IIT), Chicago, USA, 2005.
[6] A. Gierer and H. Meinhardt, A theory of biological pattern formation, Kybernetik, 12 (1972), 30-39.
[7] G. Golub and C. Van Loan, Matrix Computations, Johns Hopkins University Press, Baltimore, MA, 1996.

  [8] D. Iron, J. Wei and M. Winter, The stability of spike solutions to the one dimensional Gierer-Meinhardt model, Physica D, 150(1-2) (2001), 25-62.
  [9] A. Karageorghis and I. Kyza, Efficient algorithms for approximating particular solutions of elliptic equations using Chebyshev polynomials, Commun. Comput. Phys., 2 (2007), 501-521.
 [10] W. Lyons, H. D. Ceniceros, S. Chandrasekaran and M. Gu, Fast algorithms for spectral collocation with non-periodic boundary conditions, J. Comput. Phys., 207(1) (2005), 173-191.
 [11] H. Meinhardt, The Algorithmic Beauty of Sea Shells, Springer-Verlag, New York, 1995.
 [12] NAG Fortran library Mark 17, routine D03PCF, Numerical Algorithms Group Ltd., Oxford, United Kingdom, 1995.
 [13] W. Sun, T. Tang, M. J. Ward and J. Wei, Numerical challenges for resolving spike dynamics for two one-dimensional reaction-diffusion systems, Stud. Appl. Math., 111 (2003), 41-84.
 [14] L. N. Trefethen, Spectral Methods in MatLab, SIAM, Philadelphia, USA, 2000.
 [15] L. N. Trefethen and D. Bau, Numerical Linear Algebra, SIAM, Philadelphia, USA, 1997.
 [16] H. Van Der Vorst, Iterative solution methods for certain sparse linear systems with a non-symmetric matrix arising from PDE-problems, J. Comput. Phys., 44 (1981), 1-19.
 [17] S. Balay, K. Buschelman, V. Eijkhout, W. Gropp, D. Kaushik, M. Knepley, L. C. McInnes, B. Smith and H. Zhang, Portable, Extensible Toolkit for Scientific Computation, Version 2.3.1, Released Feb. 3, 2006, http://www-unix.mcs.anl.gov/petsc/petsc-2/.
 [18] Z. Qiao, Numerical investigations of the dynamical behaviors and instabilities for the Gierer-Meinhardt system, Commun. Comput. Phys., 3 (2008), 406-426.
 [19] Z. Qiao, Numerical solution for nonlinear Poisson-Boltzmann equations and numerical simulations for spike dynamics, Ph.D. Thesis, Hong Kong Baptist University, 2006.
 [20] M. Ward and D. Iron, The dynamics of multi-spike solutions for the one-dimensional Gierer-Meinhardt model, SIAM J. Appl. Math., 62(6) (2002), 1924-1951.
 [21] H. Meinhardt and A. Gierer, Pattern formation by local self-activation and lateral inhibition, Bioessays, 22 (2000), 753-760.
 [22] J. Wei and M. Ward, Asymmetric spike patterns for the one-dimensional Gierer-Meinhardt model: Equilibria and stability, Euro. J. Appl. Math., 13(3) (2002), 283-320.
 [23] A. Turing, The chemical basis of morphogenesis, Philos. T. Roy. Soc., 237 (1952), 37-72.
 [24] M. Ward, D. McInerney, P. Houston, D. Gavaghan and P. Maini, The dynamics and pinning of a spike for a reaction-diffusion model, SIAM J. Appl. Math., 62(4) (2002), 1297-1328.
 [25] J. Schnakenberg, Simple chemical reaction systems with limit cycle behavior, J. Theor. Biol., 81 (1979), 389-400.
 [26] D. Iron and M. Ward, Spike pinning for the Geirer-Meinhardt model, J. Math. Comput. Simul., 55 (2001), 419-431.